

Strengths of serpentinite gouges at elevated temperatures

D. E. Moore and D. A. Lockner

U.S. Geological Survey, Menlo Park, California

Ma Shengli

Institute of Geology, State Seismological Bureau, Beijing, China

R. Summers and J. D. Byerlee

U.S. Geological Survey, Menlo Park, California

Abstract. Serpentinite has been proposed as a cause of both low strength and aseismic creep of fault zones. To test these hypotheses, we have measured the strength of chrysotile-, lizardite-, and antigorite-rich serpentinite gouges under hydrothermal conditions, with emphasis on chrysotile, which has thus far received little attention. At 25°C, the coefficient of friction, μ , of chrysotile gouge is roughly 0.2, whereas the lizardite- and antigorite-rich gouges are at least twice as strong. The very low room temperature strength of chrysotile is a consequence of its unusually high adsorbed water content. When the adsorbed water is removed, chrysotile is as strong as pure antigorite gouge at room temperature. Heating to ~200°C causes the frictional strengths of all three gouges to increase. Limited data suggest that different polytypes of a given serpentine mineral have similar strengths; thus deformation-induced changes in polytype should not affect fault strength. At 25°C, the chrysotile gouge has a transition from velocity strengthening at low velocities to velocity weakening at high velocities, consistent with previous studies. At temperatures up to ~200°C, however, chrysotile strength is essentially independent of velocity at low velocities. Overall, chrysotile has a restricted range of velocity-strengthening behavior that migrates to higher velocities with increasing temperature. Less information on velocity dependence is available for the lizardite and antigorite gouges, but their behavior is consistent with that outlined for chrysotile. The marked changes in velocity dependence and strength of chrysotile with heating underscore the hazards of using room temperature data to predict fault behavior at depth. The velocity behavior at elevated temperatures does not rule out serpentinite as a cause of aseismic slip, but in the presence of a hydrostatic fluid pressure gradient, all varieties of serpentine are too strong to explain the apparent weakness of faults such as the San Andreas.

Introduction

Serpentinite is closely associated with oceanic transform faults [Christensen, 1972; Bonatti, 1976; Francis, 1981], which are interpreted to be mechanically weak [Oldenberg and Brune, 1975; Wilcock *et al.*, 1990] and in some cases to have a component of aseismic slip [Engeln *et al.*, 1986]. Within the San Andreas system, serpentinite has been linked with the fault sections of central California that show creep [e.g., Allen, 1968; Irwin and Barnes, 1975], although geophysical evidence for extensive serpentinite bodies at depth in those sections is lacking [Wang, 1984]. Nevertheless, serpentinite-bearing fault zone materials have been mapped in the creeping section of the San Andreas fault [Rymer, 1982], and serpentinite gouge has been collected from shallow trenches in the San Andreas and Hayward faults [Morrow *et al.*, 1982; Moore *et al.*, 1986]. Recent experimental studies have suggested the possibility that certain types of serpentinite might explain both aseismic slip and low shear strength of faults [Reinen *et al.*, 1991, 1993; Reinen and Tullis, 1995]. Evaluation of this hy-

pothesis requires that we understand how serpentinite-bearing faults will behave at depth. Because previous strength measurements on serpentinite have principally been conducted at room temperature on dry samples, we have investigated the strength of serpentinite gouges at elevated temperatures and under controlled conditions of fluid pressure.

The mineral group serpentine, with end-member composition $\text{Mg}_3\text{Si}_2\text{O}_5(\text{OH})_4$, principally forms as a replacement of the olivine and pyroxenes of ultramafic igneous rocks at temperatures below about 500-600°C [Evans *et al.*, 1976] and in the presence of water. Serpentine is a 1:1 sheet silicate, in which a given sheet consists of an Si-bearing tetrahedral layer that is joined to an Mg- and OH-bearing octahedral layer by sharing oxygens (for a comprehensive review of serpentine mineralogy, see Wicks and O'Hanley [1988]). The lateral dimensions of an ideal Mg-bearing octahedral layer are larger than those of an ideal Si-bearing tetrahedral layer, and the resulting stresses between these layers give rise to three major varieties of serpentine (lizardite, antigorite, and chrysotile), each reflecting a different adjustment to the structural problem. Lizardite maintains a platy form by stretching the tetrahedral layer and compressing the octahedral layer to make the sheet structure lie flat. The sheet structure of chrysotile curls around to form hollow tubes, with the smaller tetrahedral layer on the inside. Antigorite has an alternating curved structure that pro-

This paper is not subject to U.S. copyright. Published in 1997 by the American Geophysical Union.

Paper number 97JB00995.

duces a corrugated or wavy pattern; a given tetrahedral layer is tied to the octahedral layer above it for half a wavelength and tied to the one below it for the other half. Adjacent sheets in lizardite and chrysotile are linked by relatively weak bonds between the hydrogen ions at the top of the octahedral layer and the basal oxygens of the overlying tetrahedral layer. Both chrysotile and lizardite can occur in a number of polytypes, representing different stacking arrangements of the sheets [Whittaker and Zussman, 1956; Bailey, 1988; Bailey and Banfield, 1995].

Antigorite is the high-temperature form of serpentine, being stable from about 200°C to 500–600°C under crustal conditions [Evans *et al.*, 1976]. Chrysotile and lizardite are both low-temperature varieties; their upper thermal stability limit may be 250–300°C, suggested by field relationships [e.g., Coleman, 1971; Evans *et al.*, 1976] and oxygen-isotope-fractionation studies [Wenner and Taylor, 1970; O'Hanley and Wicks, 1995; O'Hanley, 1996]. O'Hanley *et al.* [1989] suggested that lizardite may form metastably under conditions of low water pressure and subsequently be replaced by chrysotile if water pressure increases. This is consistent with the observation that chrysotile most commonly forms as a replacement of other serpentine minerals [O'Hanley *et al.*, 1989; O'Hanley, 1991] rather than as a direct replacement of olivine or pyrox-

ene. More recently, however, O'Hanley and Wicks [1995] and O'Hanley [1996] proposed that lizardite and chrysotile may be stable under different chemical conditions at a given temperature and pressure.

All three serpentine minerals are therefore of potential significance to fault zones, and a gouge rich in each variety was tested in this study. Antigorite will be the stable form at depths greater than ~9–10 km, depending on the local temperature gradient, although it commonly persists metastably at shallower depths because of sluggish reaction rates [e.g., Evans *et al.*, 1976]. Lizardite and/or chrysotile will be common in the upper levels of a fault zone. Natural serpentinite gouges from the San Andreas and Hayward faults are typically mixtures of lizardite and chrysotile [Moore *et al.*, 1986, 1996a]. The chrysotile content of sheared serpentinite in California is higher than that of nearby unsheared serpentinite [Page, 1968; Coleman and Keith, 1971; Mumpton and Thompson, 1975]. This increase probably reflects the large fluid volumes that are channeled through shear zones and that promote chrysotile formation by means of solution-precipitation reactions [Mumpton and Thompson, 1975; Craw *et al.*, 1987; O'Hanley, 1991]. Over time, therefore, chrysotile should be increasingly important to serpentinite-bearing faults.

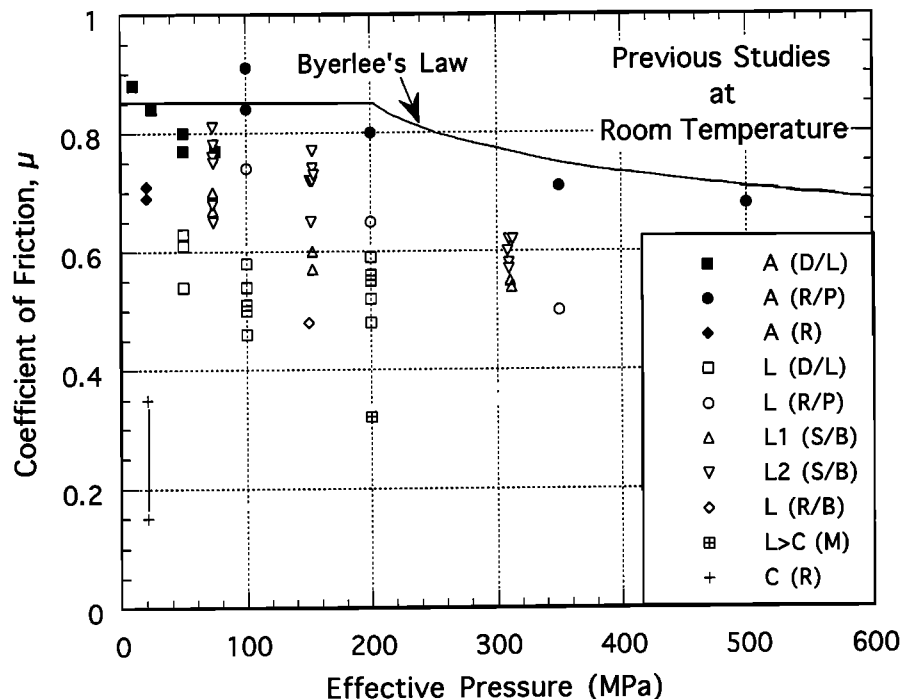


Figure 1. Plots of coefficient of friction, μ , versus effective pressure (confining pressure – fluid pressure) from previous strength investigations on serpentinite. Abbreviations are D/L, *Dengo and Logan* [1981], A is 84% serpentine, mostly antigorite, 10% oxides, and 6% magnesite and dolomite and L is 70% serpentine, mostly lizardite, 11% enstatite, and 19% oxides. R/P, *Raleigh and Paterson* [1965], A is an antigorite-rich serpentinite with 5–10% olivine, 10% magnetite, and 2% magnesite and L is a partly serpentinized peridotite with 40% serpentine, mostly lizardite, and 60% olivine and enstatite. S/B, *Summers and Byerlee* [1977b], L1 (their sample ALM-1) is 85% serpentine, mostly lizardite 6T, 13% magnetite, and 2% spinel and L2 (DP-2) is 70% serpentine, mostly lizardite 1T, 19% olivine, 8% magnetite, and 3% diopside [Moore *et al.*, 1996a]. R, *Reinen et al.* [1994], A is 90% serpentine, mostly antigorite, 5% magnetite, and 5% magnesite and C is clinochrysotile with traces of magnetite. R/B, *Rutter and Brodie* [1988], L is 70% serpentine, mostly lizardite, and 30% clinopyroxene and orthopyroxene. M, *Morrow et al.* [1982], L>C ("Golden Gate Bridge") contains lizardite 1T, clinochrysotile, and magnetite [Moore *et al.*, 1996a].

Previous Studies

Earlier triaxial frictional strength investigations on serpentinite have principally consisted of room temperature measurements made almost exclusively on lizardite- and antigorite-rich samples (Figure 1). Overall, antigoritic serpentinite has a room temperature coefficient of friction, μ , in the range 0.6–0.9, and lizardite-rich samples have $\mu = 0.45$ –0.80. These ranges overlap to a considerable degree, but when results from a single laboratory are compared, antigorite-rich serpentinites are consistently stronger than lizardite-rich ones [Raleigh and Paterson, 1965; Dengo and Logan, 1981]. The wide range of lizardite strengths in part reflects different degrees of preservation of relict minerals. The stronger lizardite samples generally contain several percent pyroxene \pm olivine; for example, the stronger of two lizardite-rich samples examined by Summers and Byerlee [1977b] contains relict pyroxenes and olivine, whereas the weaker one does not. The coefficient of friction of both lizardite- and antigorite-rich serpentinites decreases with increasing effective pressure; Raleigh and Paterson [1965] attributed this effect to increased ductility of serpentinite at high pressures.

The frictional strength of chrysotile serpentinite has only recently been considered. Reinen *et al.* [1993] reported a very low coefficient of friction for chrysotile, at 0.20–0.25, in marked contrast to the much stronger lizardite and antigorite serpentinites. A second chrysotile sample (this material was originally identified as lizardite [Reinen *et al.*, 1994] but subsequently determined to be chrysotile [Reinen and Tullis, 1995]) is also weak, with μ in the range 0.15–0.35 (Figure 1). The strength of a mixed, lizardite + chrysotile-bearing gouge tested by Morrow *et al.* [1982] plots at the upper end of the chrysotile range in Figure 1.

Few studies have been conducted on heated serpentinite samples. Raleigh and Paterson [1965] measured serpentinite strength at temperatures to 700°C, but most of their experiments were conducted in closed systems, in which water released during dehydration reactions at temperatures above 300–500°C substantially decreased the effective pressure and consequently the strength. In contrast, one vented, heated sample remained relatively strong. Rutter and Brodie [1988] determined that the strength of a lizardite-rich serpentinite was higher at 300°C than 20°C, under controlled conditions of fluid pressure. Similarly, Moore *et al.* [1983, 1986] reported a strength increase between 200 and 400°C for a natural serpentinite gouge containing roughly equal amounts of lizardite and chrysotile. These few data suggest that lizardite- and antigorite-bearing serpentinites may maintain or increase their strength upon heating; however, it has been suggested that increasing temperature might lower the strength of chrysotile [Reinen *et al.*, 1993].

Sample Descriptions

The samples used in this study are described briefly below; more thorough descriptions are provided by Moore *et al.* [1996a]. Mineral proportions (Table 1) were determined by point counts of thin sections. Serpentine-mineral identifications were based on X ray powder diffraction analysis, with reference to the crystallographic data presented by Whittaker and Zussman [1956] and Wicks and O'Hanley [1988]. Natural serpentinites commonly contain more than one serpentinite mineral, but the coincidence of many of the principal X ray

Table 1. Mineral Proportions of Serpentinite Samples

	Chrysotile	Antigorite	Lizardite
Serpentine	100.0	76.0	93.0
Calcite		7.8	
Chlorite		2.9	0.3
Magnetite		12.5	5.4
Ni-sulfide*		0.3	
Chromite		0.5	
Spinel			1.3
Ilmenite			Tr
Mn-oxide*			Tr

In volume percent; Tr is trace amount.
*Elements identified in SEM.

peaks makes it almost impossible to identify a minor serpentinite constituent by bulk X ray techniques if it comprises less than 10% of a sample [Faust and Fahey, 1962].

Chrysotile

The sample is a soft, layered, grayish-green rock from New Idria, California, provided by R. G. Coleman. It is essentially all serpentine (Table 1), and X ray analysis combined with petrographic observations suggest the sole presence of clinochrysotile, which is the most important polytype of chrysotile [Whittaker and Zussman, 1956].

Lizardite

The specimen is a thoroughly serpentinitized peridotite, fine-grained overall and dark greenish brown in color, from Gold Beach, Oregon. It contains more than 90% serpentine, with magnetite the principal accessory mineral (Table 1). Sample preparation consisted of the removal of pale bluish-green veins and blue-green altered rock, which were suspected of being chrysotile. The X ray pattern of the separate is consistent with lizardite 1T, the most commonly occurring lizardite polytype [Wicks and O'Hanley, 1988].

Antigorite

The source material is a large, grayish to brownish black resistant block from the KCAC, Inc. asbestos mine near New Idria, California. It is the least pure of the three serpentinite samples, containing about 75% serpentine along with magnetite, calcite, and chlorite (Table 1). The numerous light green chrysotile veins and surface coatings were removed as much as possible from the sample prior to grinding. Although antigorite is the only serpentinite mineral to appear on the X ray pattern, the sample undoubtedly contains at least a few percent chrysotile and possibly some lizardite. This material would be representative of serpentinites that have been altered by migrating groundwaters in a fault zone.

Other Samples

L. Reinen and T. Tullis generously provided some of the chrysotile [Reinen and Tullis, 1995] gouge T91NI6, examined by Reinen *et al.* [1994], to conduct an interlaboratory comparison of reported strengths. An X ray diffraction pattern of T91NI6 reveals only clinochrysotile peaks [Moore *et al.*, 1996a], but small amounts of magnetite are visible in thin section. Single room temperature experiments were conducted on

two additional gouge samples: one is a clear yellow serpentine mineral from Cape San Martin, California, whose X ray pattern is consistent with orthochrysotile, one of the less abundant polytypes of chrysotile [Whittaker and Zussman, 1956]. The other sample is a mottled, yellow to pale gray serpentinite from New Idria, California, containing lizardite 1T and lesser amounts of clinochrysotile.

Experimental Methods

The experimental apparatus (Figure 2) differs in only a few details from the assembly used in our earlier high temperature strength investigations [e.g., Moore *et al.*, 1983, 1986, 1989]. The prepared serpentinite samples, including T91NI6 [Reinen *et al.*, 1994], were ground by hand and passed through an 88- μm sieve, to produce simulated gouges. For the strength tests, a 1-mm-thick layer of gouge was placed along a 30° sawcut in a 19.1-mm-diameter cylinder of antigoritic serpentinite (Figure 2), obtained from the same source as that for the antigorite-rich gouge. The sawcut surfaces were roughened with #60 SiC prior to sample assembly. A borehole for pore fluid entry was drilled all the way through the upper piece of the cylinder (Figure 2) to ensure that the gouge did not become isolated from the pore fluid system. The borehole was packed with quartz beads, which allowed free flow of fluid but minimized the extrusion of gouge into the borehole. As a test of pore fluid communication, at the end of two heated experiments, pore pressure and normal stress were increased together by about 5 MPa (1 MPa = 10 bars) from the starting values of 10 (pore pressure) and 110 MPa (normal stress). In both cases, there was almost no change in shear strength measured at 0.2 $\mu\text{m/s}$ axial velocity, as expected for a sample in good hydraulic communication with the external pore pressure system.

The assembled samples were housed in annealed copper jackets to separate them from the confining pressure medium. Reported strengths in this paper have been corrected for the strength of the copper jackets, which contribute a significant proportion of the measured strengths. Details of the correction procedure are presented by Moore *et al.* [1996a]. In brief, the room temperature correction involved a comparison of copper and polyurethane jacket strengths, using samples prepared by substituting a sheet of teflon for the gouge layer and steel end pieces for the antigorite cylinder. At room temperature, a first-order jacket shear strength correction of $\tau_{\text{jacket}} = 10.2 \text{ MPa} + 1.94Z$ was applied to the strength data, where Z is the amount of axial shortening in millimeters. Calibration runs showed that this correction matched the jacket strength to ± 2 MPa. The copper jacket becomes progressively softer with increasing temperature, and the temperature dependence of the correction factor was estimated from additional teflon/steel experiments. Teflon should be stable for the length of the experiments at all temperatures tested.

Confining pressure was applied first to the sample, followed by the pore pressure, with deionized water as the pore fluid. Confining pressure was measured to within 0.02 MPa, at an accuracy of ± 0.3 MPa. Pore pressure was also measured to a precision of 0.02 MPa and ± 0.2 MPa accuracy. After the pressures had equilibrated, the temperature was raised to the desired value. Temperature was monitored by a thermocouple inserted along the pore pressure inlet. The samples were positioned in the furnace such that the temperature maximum, as then determined, was located near one end, with temperature decreasing

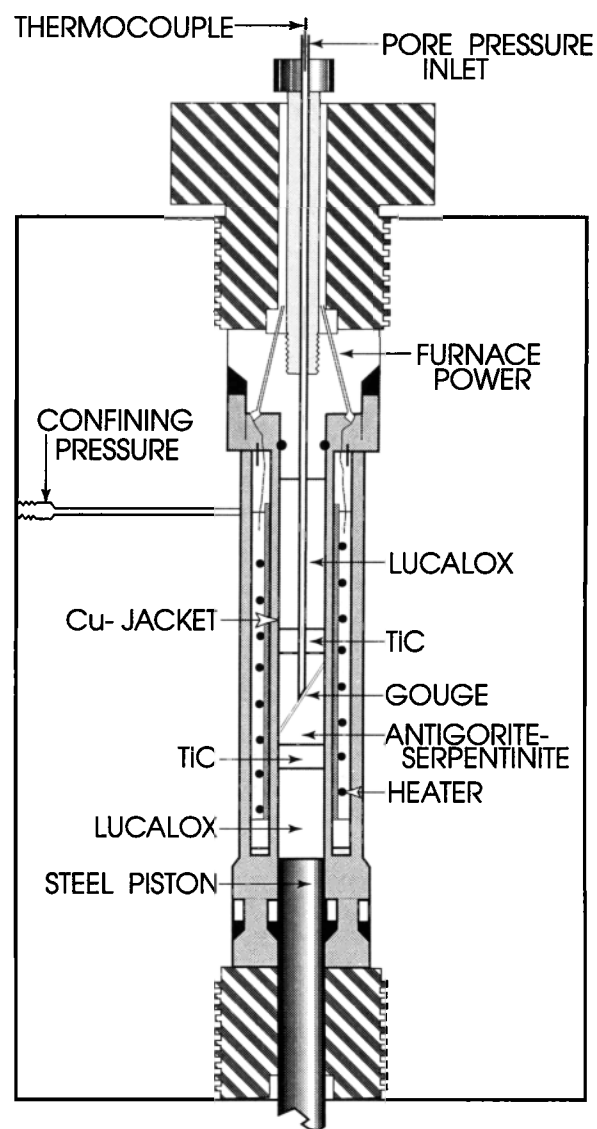


Figure 2. Triaxial friction apparatus for experiments at elevated temperatures.

by 2% across the length of the samples. After these experiments were completed, however, we discovered that the position of the peak temperature along the length of the furnace varies with the pressure of the argon gas that was used as the confining-pressure medium. For the range of confining pressures applied in this study, the actual temperatures along the samples were $\sim 3\%$ lower than we thought. Corrected temperatures are used throughout this paper.

All experiments were run at a constant normal stress, which was maintained by means of computer-controlled adjustments to the confining pressure. Axial stress was measured to a precision of 0.1 MPa and an accuracy of 1.0–1.5 MPa, and displacement measurements were made to a precision of 0.1 μm and an accuracy of approximately 5.0 μm . The machine stiffness is equivalent to 495 MPa/mm shear stress for a 19.1-mm-diameter sample. Corrections for changes in contact area along the sliding surface were made according to the calculations presented by Scott *et al.* [1994]. The absolute value of seal friction was zeroed out before a given sliding test com-

menced. Because seal friction is a function of confining pressure, an additional correction was applied during the experiment to account for the continuing adjustments to confining pressure to maintain a constant normal stress. The overall correction for the seal friction is about 1% of the value of confining pressure.

Combining all sources of error, a reported value of frictional strength is estimated to be accurate to within 10%. Relative changes in friction will have much better accuracy because velocity steps were made within a single experiment.

Results

Strength Measurements

Strengths at different temperatures and sliding velocities for our three serpentinite gouges and for T91Ni6 are plotted in Figures 3–5, in which the coefficient of friction, μ is shear stress divided by effective normal stress. These experiments

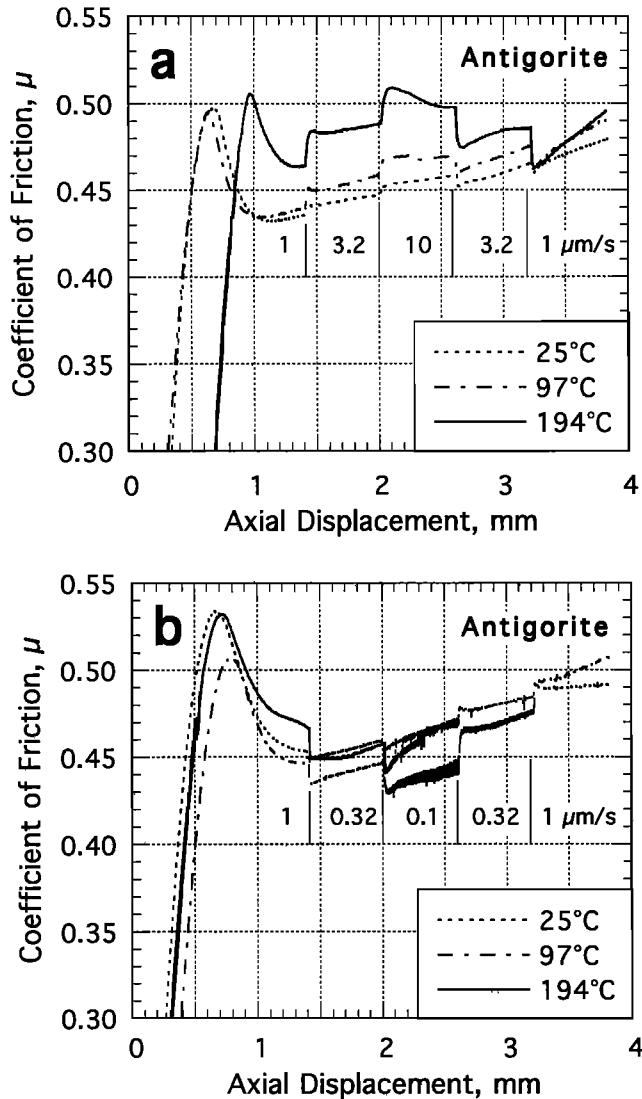


Figure 3. Coefficient of friction of the antigorite-rich gouge to 194°C as a function of displacement and sliding rate, at 100 MPa effective normal stress; (a) fast (1–10 $\mu\text{m/s}$) and (b) slow (0.1–1.0 $\mu\text{m/s}$) axial velocities.

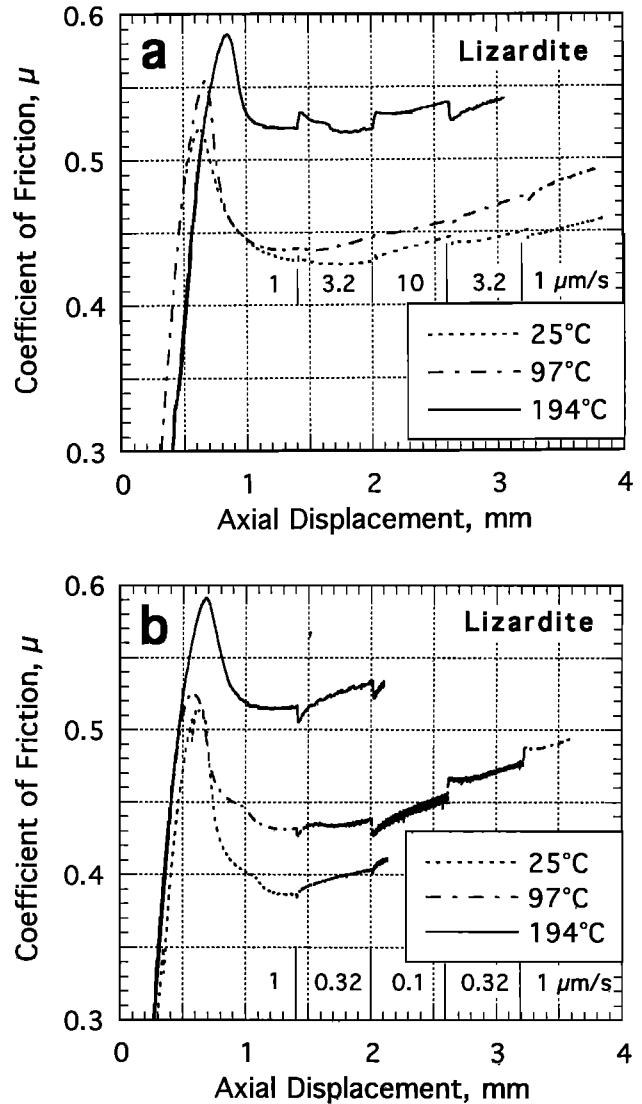


Figure 4. Coefficient of friction of the lizardite gouge in the range 25–194°C at 100 MPa effective normal stress; (a) fast (1–10 $\mu\text{m/s}$) and (b) slow (0.1–1.0 $\mu\text{m/s}$) axial displacement rates.

were all run at a pore pressure of 10 MPa and a normal stress of 110 MPa, to yield an effective normal stress of 100 MPa. The velocities indicated in the figures are axial velocities, corresponding to the rate of advance of the piston (Figure 2). Nominal slip rates along the inclined sawcut (Figure 2) would be 15.5% higher than the axial velocities. All of the experiments are characterized by stable slip, and their strength behavior follows similar overall trends. The coefficient of friction increases initially to a peak value at 0.5–1 mm axial displacement for antigorite and lizardite (Figures 3 and 4) and 0.3–0.5 mm for the two chrysotile samples (Figures 5a and 5b). The coefficient of friction then decreases by as much as 0.1, after which it levels off or gradually increases again as a result of strain hardening. The final value of μ in some experiments reaches or even exceeds the early peak value. Changes in μ accompanying the velocity steps are superimposed on this overall trend. In many cases a given gouge sample is relatively strong at 10 $\mu\text{m/s}$ (Figures 3a, 5a, and 5b) and relatively weak at 0.1 $\mu\text{m/s}$ (Figures 3b and 5a). However,

in several other experiments, such as the 25 and 97°C lizardite experiments in Figure 4a, a velocity effect is hardly noticeable. Quantitative consideration of velocity effects is treated in a subsequent section.

The antigorite- and lizardite-rich gouges have coefficients of friction in the range 0.4–0.6 (Figures 3 and 4). The room temperature values for the lizardite gouge are consistent with previous measurements made on lizardite samples that lack relict minerals, but the antigorite-rich gouge is rather weaker than previously studied antigorite serpentinites (Figure 1), probably because of the large amount of other minerals in the sample. In contrast, the two chrysotile gouges are only about one-half as strong as the lizardite and antigorite-rich gouges. The room temperature results for sample T91NI6 are consistent with those obtained for that gouge by *Reinen et al.* [1994], indicating that reported strengths from the two laboratories are directly comparable. In identical experiments (Figure 5c), the strengths of the two polytypes orthochrysotile and clinochrysotile initially follow slightly different trends but coincide after about 2.5-mm displacement. Lizardite strength clearly increases with temperature (Figure 4), whereas the curves at different temperatures for the antigorite (Figure 3) and chrysotile (Figure 5) gouges overlap to a considerable degree.

Figure 6 compares the value of μ at 3.4 mm displacement (and a velocity of 1 $\mu\text{m/s}$) for each experiment in Figures 3–5, with additional data from *Moore et al.* [1996a]. Experiments in which the slowest velocity interval was 1.0 $\mu\text{m/s}$ are represented by open symbols, whereas experiments containing a velocity step at 0.1 $\mu\text{m/s}$ are indicated by solid symbols. For all three gouge types, "slow" experiments plot at higher values of μ than "fast" experiments. These differences suggest the operation of a time-dependent strengthening process that is independent of the changes in μ associated with the velocity steps. A good example is the 194°C chrysotile experiment in Figure 5a, in which μ drops to lower values at each step change in velocity between 10 and 0.1 $\mu\text{m/s}$ due to rate dependence, but the increase in μ with displacement is greater during the intervals at 0.1 and 0.32 $\mu\text{m/s}$ than at faster velocities. The trend lines in Figure 6 confirm the marked increase in lizardite strength with increasing temperature and suggest a slight increase for chrysotile and antigorite, as well. Chrysotile sample T91NI6 follows a similar trend relative to temperature as our chrysotile gouge but at slightly higher values of μ . T91NI6 may contain undetected amounts of one or both of the stronger serpentine minerals lizardite and antigorite. The strength of the sample rich in both lizardite and chrysotile (L>C) is intermediate between the chrysotile and lizardite gouge strengths.

As noted previously, at 97 and 194°C chrysotile strength shifts to progressively lower values as velocity steps downwards from 10 to 0.1 $\mu\text{m/s}$ (Figure 5a). To determine whether further strength reductions would occur at even lower velocities, heated chrysotile experiments were run at axial velocities as low as 0.001 $\mu\text{m/s}$, which corresponds to a slip rate along the inclined sawcut surface of about 36.4 mm/yr. (The average slip rate of the San Andreas fault in central California is 33–38 mm/yr [*Thatcher*, 1990].) At 97°C, decreasing the axial velocity by steps from 1.0 to 0.001 $\mu\text{m/s}$ leads to successively smaller increments of strength decrease, to a minimum of $\mu \approx 0.15$ (Figure 7a). At 194°C, chrysotile strength is almost independent of velocity change at the slowest rates, and the sample is significantly stronger, with μ approaching 0.35 when the jacket failed. Much of the increase at 194°C is at

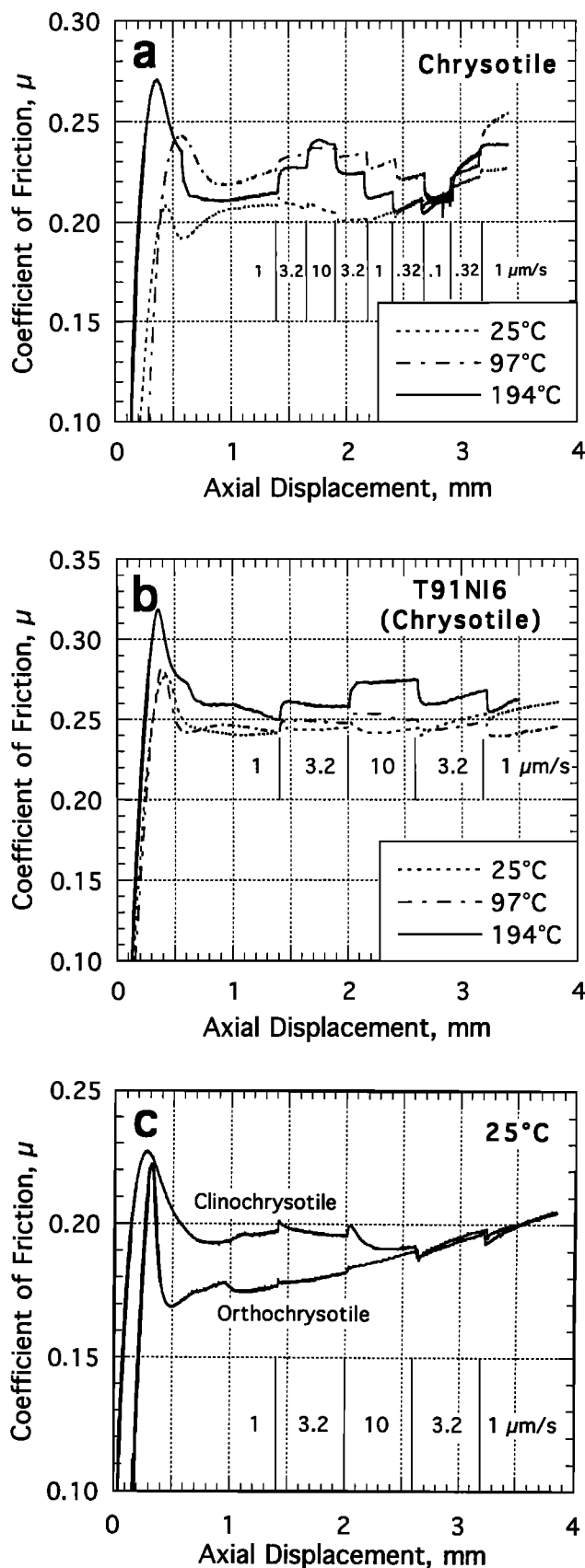


Figure 5. (a) Coefficient of friction of our clinochrysotile gouge at 0.1–10.0 $\mu\text{m/s}$ axial velocities; (b) μ of clinochrysotile gouge T91NI6 at fast (1–10 $\mu\text{m/s}$) velocities; (c) comparison of orthochrysotile and clinochrysotile strengths. Effective normal stress is 100 MPa.

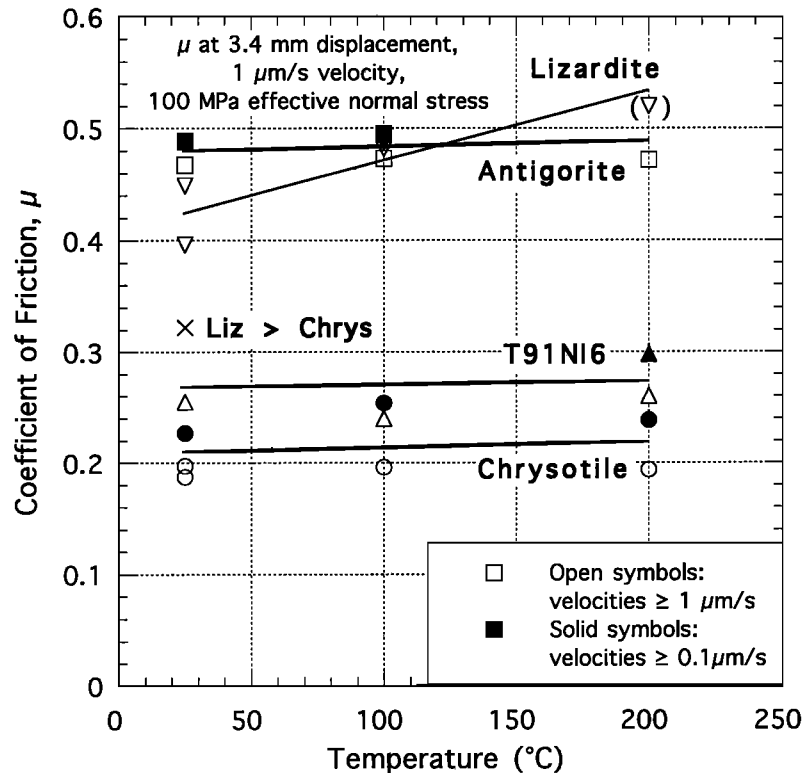


Figure 6. Comparative gouge strengths relative to temperature at 3.4 mm axial displacement and 1.0 $\mu\text{m/s}$ velocity. Circles are chrysotile gouge; triangles are T91N16 (chrysotile) gouge; inverted triangles are lizardite gouge; squares are antigorite gouge; cross is a mixed gouge containing more lizardite than chrysotile. The 194°C lizardite point in parentheses is the average of the 1 $\mu\text{m/s}$ velocity steps at 1.3–1.4 mm displacement (Figure 4); because of probable strain hardening, this point should be a lower limit for μ at 3.4 mm. Trend lines for each gouge were obtained by fitting separate lines to the slow and fast data and then averaging the two, nearly parallel lines. In the case of sample T91N16, the fit to the fast runs was shifted upward, to lie between the slow and fast points at 194°C.

tributable to a marked, time-dependent strengthening of the gouge during the interval at 0.001 $\mu\text{m/s}$. This increase is of the same type as that shown by the slow experiments in Figure 6, but here the effect is more pronounced because of the correspondingly longer time involved.

In all the experiments described thus far, the effects of velocity and temperature have been examined at constant normal stress and fluid pressure, resulting in temperature-pressure combinations that are not always representative of the conditions to be expected in a fault zone. Therefore low-velocity experiments were run on chrysotile samples at the temperature-pressure conditions corresponding roughly to depths of 3, 6, and 9 km in the San Andreas fault (Figure 7b), assuming a hydrostatic fluid-pressure gradient of 10.0 MPa/km, a surface temperature of 20°C, a geothermal gradient of $\sim 30^\circ\text{C/km}$ [Lachenbruch and Sass, 1973], a serpentinite density of 2.55 g/cm^3 [Deer et al., 1962; Coleman, 1971], and a normal stress equal to the lithostatic pressure at all depths. The latter assumption is discussed by Moore et al. [1996a]. The effective normal stress of 46.5 MPa used on the 3-km (107°C) sample is less than half that of the 97°C sample in Figure 5a, and the coefficient of friction drops to a minimum value of ~ 0.10 . The conditions of the 6-km (194°C) experiment are nearly the same as those of the 194°C experiments in Figures 5a and 7a, and the strengths are also similar. The 9-km (281°C) sample is substantially stronger, with $\mu > 0.5$; this strength is close to

that estimated for the lizardite and antigorite gouges at 281°C, extrapolated from the trends in Figure 6. Pronounced increases in μ occur during the 0.001 $\mu\text{m/s}$ step of the 6- and 9-km experiments (Figure 7b), and μ remains high during subsequent velocity intervals.

Deformation Textures

Thin sections for petrographic analysis were prepared from about half the samples. Sections were cut parallel to the cylinder axis and perpendicular to the sawcut. The other samples were disassembled principally for bulk X ray diffraction analysis, but portions of some were reserved for examination with a stereomicroscope and a scanning electron microscope (SEM).

All of the samples that were selected for X ray analysis fell apart along slickensided surfaces when the copper jackets were removed. These surfaces either follow the sawcut boundaries (boundary shears) or cross the gouge in an orientation consistent with R shears (Figure 8a). Many of the boundary shears extend only partway along the sawcut; in such cases, an R shear traverses the gouge layer from the termination point (Figure 8b). A given thin section can show traces of up to 13 R shears across the gouge layer, although some samples contain only 2 or 3 prominent R shears. Most of the R shears make angles of 12–18° to the sawcut, with an overall range of about 5–24°. No correlations were discernible between R shear orientations and experimental conditions. Relatively scarce P

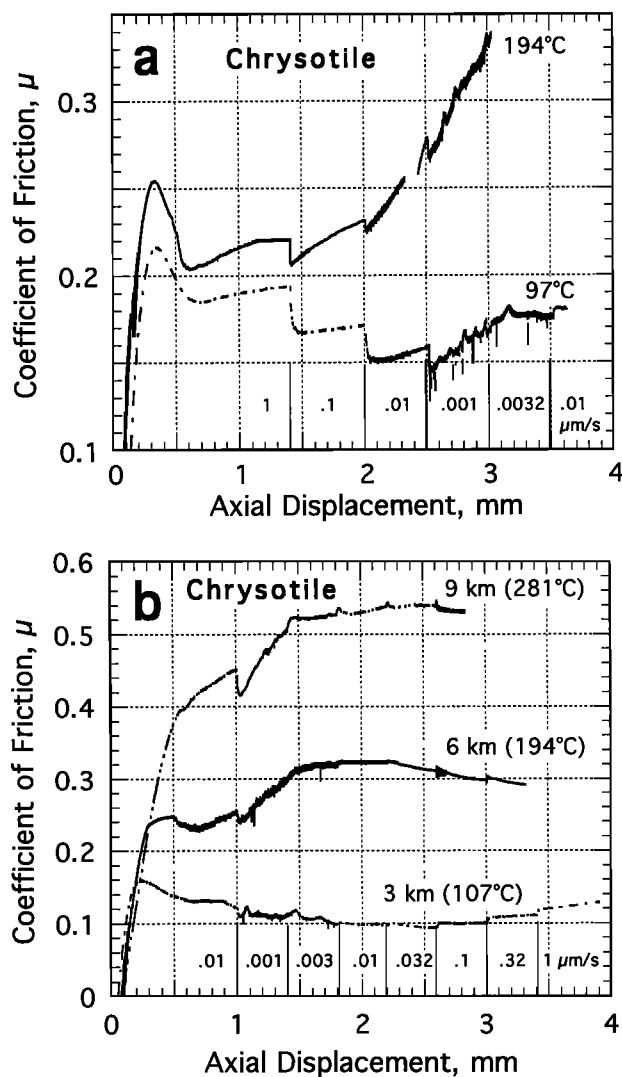


Figure 7. Coefficient of friction of heated chrysotile gouge at axial velocities as low as 0.001 $\mu\text{m/s}$. (a) Experiments at 100 MPa effective normal stress. (b) Experiments simulating depths of burial of 3, 6, and 9 km in a fault zone. 3 km = 107°C, 46.5 MPa effective normal stress (76.5 MPa normal stress and 30 MPa pore pressure); 6 km = 194°C, 93 MPa effective normal stress (153 MPa normal stress and 60 MPa pore pressure); 9 km = 281°C, 139.5 MPa effective normal stress (229.5 MPa normal stress and 90 MPa pore pressure). Transient decreases in μ at the slowest steps are caused by changes in room temperature as the air-conditioning system is turned on and off daily; these changes affect the length of the sample column between the fault and the point where axial displacement is measured.

shears form short segments connecting other shears. Many of the R and boundary shears are actually zones of anastomosing, thin shears that appear as hairline discontinuities in thin section (Figure 8c) and that form the slickensided surfaces visible in SEM (Figures 8d and 8e). The individual slip surfaces have an irregular, wavy form (Figure 8d), and the large waves are scored in turn by smaller-amplitude ridges and valleys (Figure 8e). Slip surfaces developed in all three serpentine varieties are shiny and smooth, but those in the chrysotile samples have an especially shiny, almost waxy appearance. The presence of the borehole does not obviously affect shear develop-

ment. Boundary shears cross the borehole in some samples, whereas in others the area around the borehole is not sheared.

Deformation features in all the gouge samples appear to be confined to the vicinity of the shears. Along narrow bands on either side of the boundary shears and at the sites where R and boundary shears come together, the gouge completely loses its original clastic character and acquires a well-developed foliation with a P orientation (Figure 8c). Foliated gouge adjacent to the boundary shears commonly contains rows of kink bands oriented at relatively large angles to the shear. The three gouge types remain soft to 194°C, but the one 281°C sample was more difficult to hand grind for X ray analysis. X ray diffraction analysis showed no obvious differences from the starting materials, although minute amounts of reaction, perhaps confined to the sliding surfaces, are unlikely to appear on a bulk X ray pattern. Such reactions would also be hard to identify with SEM techniques, because replacement textures would be destroyed on the slickensided surfaces and the reactions would probably involve little or no compositional change. Thus the possibility of reaction cannot be ruled out, although *Evans et al.* [1976] have noted the very sluggish nature of reactions involving the conversion of one serpentine mineral to another in laboratory experiments.

Origin of Low Chrysotile Strength

Under most of the experimental conditions tested (e.g., Figure 6), chrysotile was much weaker than either lizardite or antigorite. The unusual tubular form of chrysotile is not the direct cause of that mineral's often low strength, because the sheet-silicate mineral halloysite (7 Å), which commonly takes on a tubular habit [e.g., *Deer et al.*, 1962; *Giese*, 1988], is as strong as lizardite [*Summers and Byerlee*, 1977a, b]. Chrysotile strength is comparable to that of the swelling clays montmorillonite and vermiculite [*Summers and Byerlee*, 1977a, b; *Logan and Rauenzahn*, 1987; *Morrow et al.*, 1992], which can incorporate layers of water between sheets. This interlayer water was postulated to provide a "pseudo-pore pressure" [*Summers and Byerlee*, 1977a], such that the expanded clays had a higher fluid pressure than that imposed by free water in the pore spaces. Chrysotile is not a swelling clay, but it can have anomalously high adsorbed water contents [*Young and Healey*, 1954] compared to lizardite and especially to antigorite [*Deer et al.*, 1962]. Adsorption of water causes swelling of chrysotile fiber bundles; at 100% relative humidity at 25°C, 2.5 wt % H₂O can be adsorbed onto chrysotile, leading to a 6.7% increase in volume [*Deer et al.*, 1962]. We decided to test the possibility that adsorbed water is responsible for the reduced strength of chrysotile.

The water adsorbed onto chrysotile can be reversibly removed by heating to 175–200°C, without harming the crystal structure [*Deer et al.*, 1962]. Accordingly, a prepared chrysotile sample was held in a drying oven at 180°C, under vacuum, for about 120 hours. The sample was cooled while still under evacuation and then transferred directly from the oven to the triaxial apparatus. The strength of the dried chrysotile sample was measured at room temperature, an axial velocity of 0.2 $\mu\text{m/s}$, and a constant normal stress of 100 MPa (Figure 9). After 1.5-mm axial displacement, the shear stress was partly reduced, and water was introduced to the gouge layer at a pressure of 10 MPa. After 15 min equilibration time, the strength test was resumed at the same velocity and effective normal stress as before.

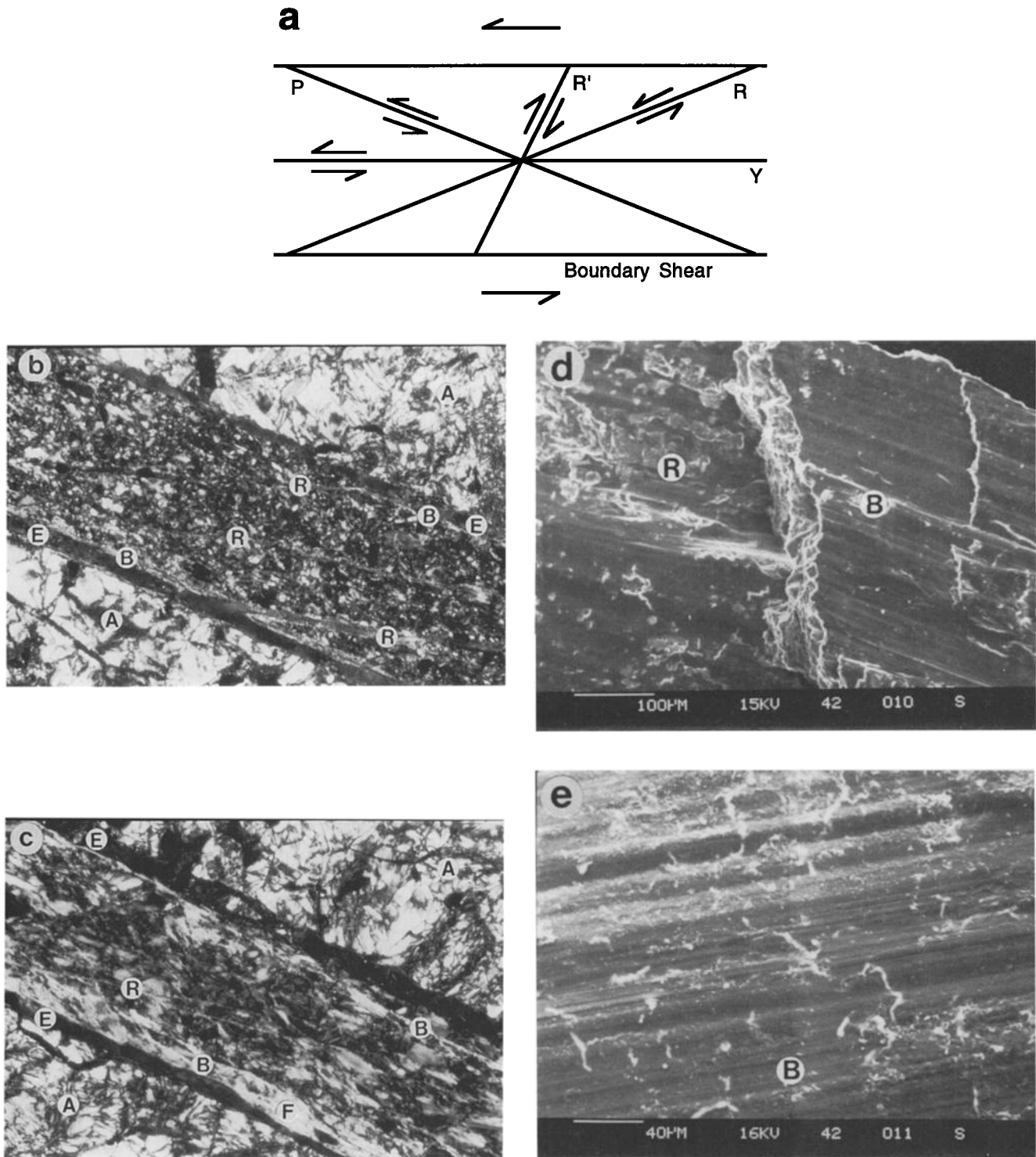


Figure 8. Gouge textures. (a) Nomenclature of commonly observed subsidiary shears within fault zones. (b) Photomicrograph showing cross section of lizardite gouge from a 97°C experiment, with narrow boundary shear (B) and well-developed R shears. The lower boundary shear is continuous across the photo, whereas the upper boundary shear only occurs to the right of the leftmost R shear. The gouge between shears retains its granular character, best illustrated by scattered magnetite grains. A is the antigorite-serpentinite cylinder; E is epoxy. (c) Photomicrograph of chrysotile gouge tested at 97°C, with a narrow upper boundary shear, a wide, composite lower boundary shear, and a band of R shears. The bright gouge within the boundary shear zone and at the junction of R and boundary shears is foliated serpentinite (F) oriented in the P direction. Gouge well away from shears consists of elongate fragments that were aligned parallel to the sawcut during sample assembly. The gouge layers in Figures 8b and 8c are now ~0.7 mm wide, as a result of compression during the experiments. (d) Secondary electron SEM photo showing slickensided surfaces of boundary and R shears in chrysotile sample T91N16, tested at 97°C. (e) Closeup of corrugated, slickensided surface of antigorite gouge from a 25°C experiment; secondary electron SEM photo.

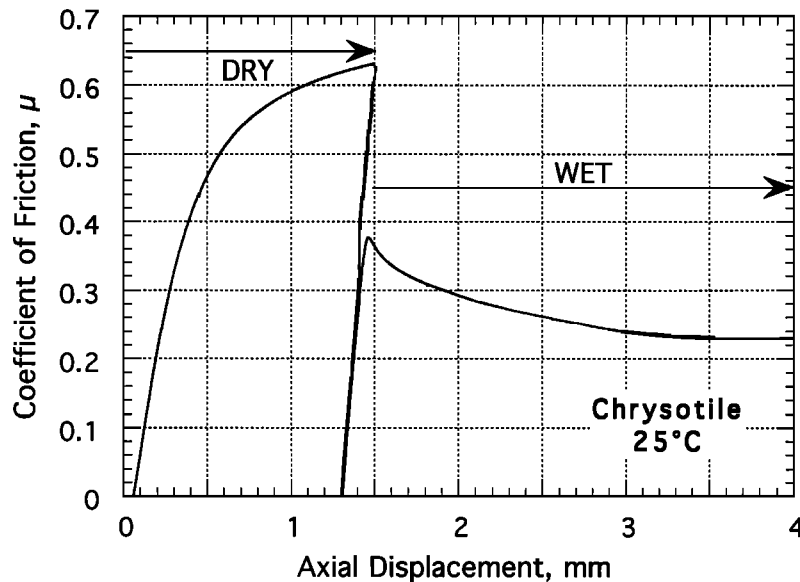


Figure 9. Comparative strength of oven-dried and wet chrysotile gouge at 25°C, 100 MPa effective normal stress, and 0.2 $\mu\text{m/s}$ axial velocity. The wet portion of the experiment was conducted at 10 MPa fluid pressure and 110 MPa normal stress.

As seen in Figure 9, the oven-dried chrysotile sample is 3 times as strong as the wet sample, and its strength was still increasing at the 1.5-mm termination of the dry run. The dry chrysotile sample has strength similar to the lizardite and antigorite serpentinites plotted in Figure 1. The coefficient of friction of the wet sample initially rose to nearly 0.4, but μ then decreased as the chrysotile equilibrated with the fluid. By the end of the experiment, μ had stabilized at about 0.23, identical to the other room temperature strengths measured for that gouge (Figure 5a). These results demonstrate that the water adsorbed onto the chrysotile fibers has a similar effect on strength as the interlayer water of swelling clays.

The number of water interlayers in montmorillonite, and consequently its strength, is a function of the effective stress [Bird, 1984]. Consistent with this, Morrow *et al.* [1992] found that μ increases with increasing effective pressure for montmorillonite but not for the nonswelling clay illite. Chrysotile strength may also increase with effective normal stress, as the adsorbed water is progressively squeezed out of the chrysotile fiber bundles at higher stress levels. The 3-km (107°C) experiment on chrysotile (Figure 7b) was conducted at about one-half the effective normal stress of the 97°C experiments (Figures 5a and 7a), and the corresponding range of μ for the 3-km sample was also about 30% lower. The 9-km (281°C) experiment was conducted at the highest effective normal stress used in this study (139.5 MPa), and the substantially greater strength of that sample may be as much a function of the increased effective normal stress as of the higher temperature. If so, chrysotile behavior contrasts with that of the other serpentine minerals (Figure 1) as well as most other minerals, because μ generally decreases somewhat with increasing normal stress [Paterson, 1978]. The possible pressure dependence of chrysotile strength is currently being investigated [Iwata *et al.*, 1996].

Velocity Dependence of Shear Strength

The data plotted in Figures 3–5 and 7 suggest varying velocity dependence of gouge strength. The sliding rate sensitivity

of shear strength is represented by the change in "steady state" coefficient of friction, $\Delta\mu_{ss}$, resulting from an exponential change in velocity: $\Delta\mu_{ss}/\Delta\ln V$. Corrections for the absolute value and the pressure dependence of seal friction had already been applied to the strength data; however, seal friction is also a function of velocity. The velocity dependence of seal friction was verified at the beginning of each experiment by means of a velocity step that was made before the piston reached the sample. A nominal correction $\Delta\mu_{seal}/\Delta\ln V = 0.0009$ has been subtracted from all reported values.

As described previously, most of the strength plots show an overall trend of increasing μ with displacement and time, and much of the uncertainty in determinations of $\Delta\mu_{ss}/\Delta\ln V$ arises from difficulties in separating the velocity and strain-hardening effects. To account for these uncertainties, an error estimate was assigned to each measurement of $\Delta\mu_{ss}$. In addition, because the choice of $\Delta\mu_{ss}$ can be a subjective process, separate sets of calculations were made by two of the authors. The individual data sets [Moore *et al.*, 1996a] are very similar. For this paper, we averaged the two sets of results, and the corresponding error estimates maximize the range of error for a given pair of data points [Moore *et al.*, 1996a]. The average values of $\Delta\mu_{ss}/\Delta\ln V$ are plotted at the midpoints of the velocity steps, in terms of axial-shortening rates, on a log scale in Figures 10–13.

The room temperature results for our chrysotile gouge and the T91NI6 chrysotile sample are essentially identical (Figure 10), and they duplicate the velocity effects reported by Reinen *et al.* [1994] for T91NI6. At moderate to high velocities, the coefficient of friction of chrysotile gouge decreases slightly with increasing velocity; such a trend is referred to as velocity weakening. In contrast, at low velocities, chrysotile is strongly velocity strengthening (μ increases with increasing velocity). The transition occurs between velocities of 0.32 and 1.0 $\mu\text{m/s}$. Raising temperature leads to marked and possibly systematic changes in velocity behavior. The trend of the 97°C data resembles a bell-shaped curve of velocity-strengthening behavior that peaks between 0.1 and 0.32 $\mu\text{m/s}$ velocity

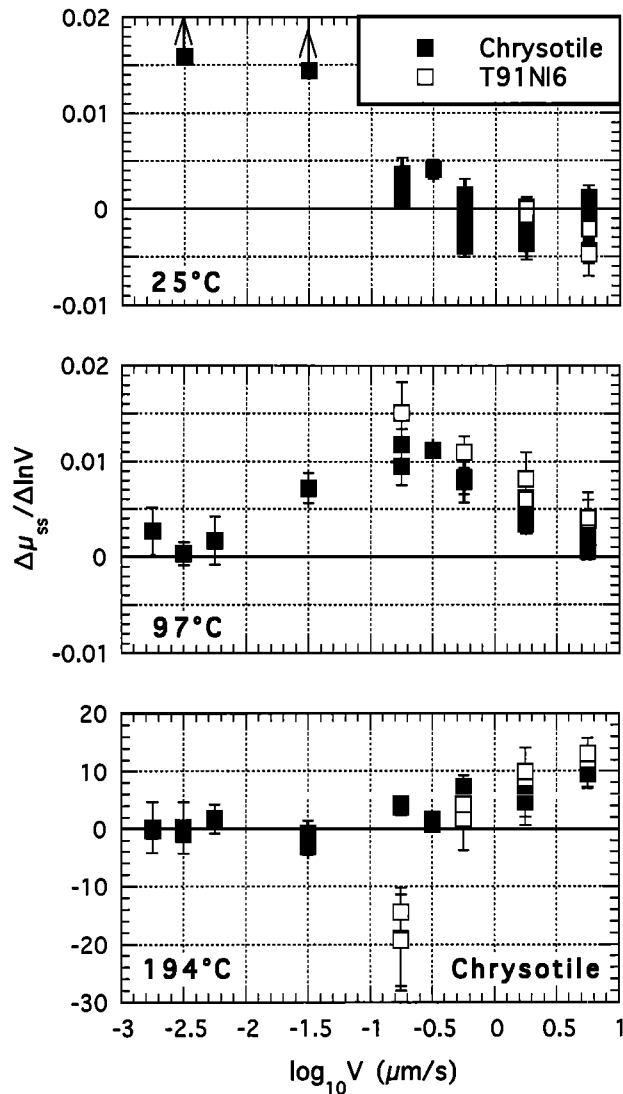


Figure 10. Steady state velocity dependence of the frictional strength of two chrysotile gouges versus log axial velocity, at 100 MPa effective normal stress.

and levels off at 0 change in μ . By comparison, the 25 and 194°C results could be interpreted as showing portions of the bell-shaped curve, with the peak migrating toward higher velocities with increasing temperature. Additional experiments at both higher and lower velocities are required to test this interpretation. The sole exceptions to the otherwise consistent results for chrysotile are the large negative values of $\Delta\mu_{ss}/\Delta\ln V$ for T91Ni6 at 194°C and a velocity step between 0.1 and 0.32 $\mu\text{m/s}$. The three aberrant data points were obtained from two separate experiments.

Velocity dependence data for the 3-, 6-, and 9-km simulation experiments on chrysotile (Figure 11) follow similar trends to those in Figure 10. The 194°C results are nearly identical, as expected from the very similar experimental conditions. The peak of velocity-strengthening behavior at 107°C appears to be displaced to higher velocities relative to the 97°C curve for chrysotile. This shift could be a function of the 10°C increase in temperature, because the direction of change is consistent with the temperature trends in Figure 10. The 107°C experiment was also conducted at a relatively low effective normal

stress of 46.5 MPa, although changes in normal stress between 0 and 100 MPa may have little effect on the rate dependence of serpentinite strength [Reinen *et al.*, 1991]. Almost all of the 281°C results are in the velocity-weakening field, and they constitute the most strongly negative values that we obtained for chrysotile. The results in Figure 11 suggest a shift toward velocity-weakening behavior at higher temperature and/or effective stress conditions.

In general, the velocity data for antigorite (Figure 12) are similar to those for chrysotile (Figure 10) over the limited range tested. The 97°C results, in particular, are nearly identical for the two serpentinite gouges. The 25°C antigorite plot includes data from experiments at 50 and 100 MPa effective normal stress, and their trends overlap. The data are shifted to slightly more positive values compared both to the chrysotile results and to those for antigorite at 100 MPa normal stress reported by Reinen *et al.* [1991]. The 194°C trend is somewhat ambiguous, because of the wide scatter of the data points; however, a peak of velocity-strengthening behavior could be situated between 1.0 and 3.2 $\mu\text{m/s}$ velocity.

The velocity behavior of lizardite (Figure 13) is even more problematical, because of the common lack of repeatability. Nevertheless, lizardite can be considered to follow the same general trends as chrysotile (Figure 10), although shifted toward more velocity-weakening behavior. Of the three serpentinite gouge types, the lizardite gouge yielded the largest proportion of negative values of $\Delta\mu_{ss}/\Delta\ln V$. Also plotted in Figure 13 are room temperature values of $\Delta\mu_{ss}/\Delta\ln V$ for the mixed gouge containing more lizardite than chrysotile. Although lizardite is the most abundant mineral in the gouge, the velocity dependence of this gouge may correspond somewhat more closely to chrysotile (Figure 10), particularly at the slowest velocity step tested.

Reinen *et al.* [1992, 1994] postulated that the room temperature rate dependence of antigorite and chrysotile (T91Ni6) could be explained by a two-mechanism model, in which a state-variable constitutive law is the controlling mechanism at high velocities and a flow constitutive law is predominant at low velocities. As best illustrated by chrysotile (Figure 10), our room temperature data are consistent with their model in

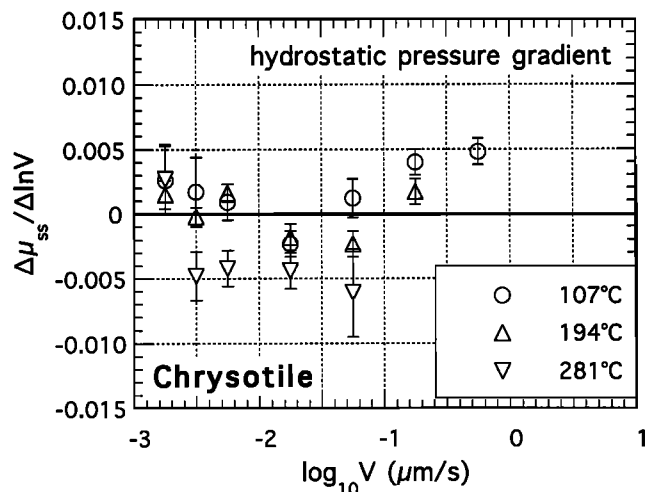


Figure 11. Steady state velocity dependence of μ for our chrysotile gouge, from experiments simulating different depths in a fault: 107°C — 3 km; 194°C — 6 km; 281°C — 9 km (see Figure 7b).

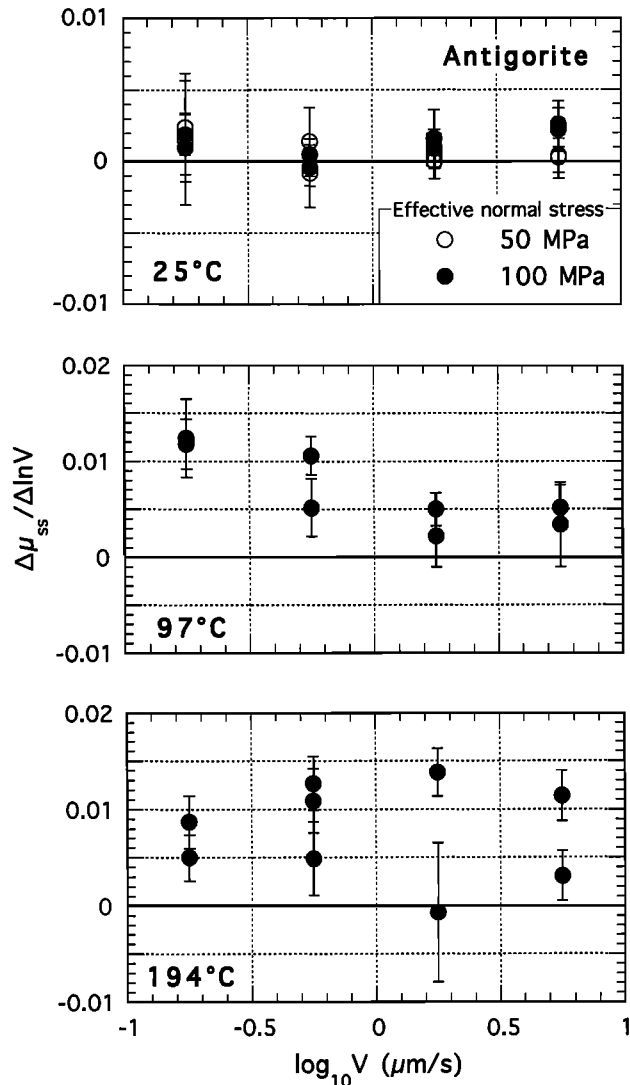


Figure 12. Velocity dependence at different temperatures of the coefficient of friction of the antigorite-rich gouge.

that velocity-strengthening behavior at slow velocities gives way to velocity-weakening behavior at fast velocities. However, their model may require some modification to explain the changing velocity dependence of chrysotile with heating.

Discussion: Significance for Fault Zones

Studies of heat flow and stress orientation around the San Andreas fault indicate that the fault is extremely weak. *Brune et al.* [1969] and *Lachenbruch and Sass* [1980] found no evidence for a heat flow anomaly directly over the fault which, combined with seismic stress considerations, led both groups to propose that the average shear strength of the fault does not exceed 20 MPa. Subsequently, *Mount and Suppe* [1987] and *Zoback et al.* [1987] determined that the maximum principal stress is nearly perpendicular to the San Andreas fault, which also implies low shear strength. In another example, *Wilcock et al.* [1990] concluded that the least principal stress is nearly perpendicular to the strike of the transform portion of the Kane Fracture Zone associated with the Mid-Atlantic Ridge, which also suggests a low level of shear stress resolved on that fault.

Two principal groups of models have been invoked to explain this weakness: (1) The fault zone contains very low-strength materials. (2) Fluid pressures within the fault zone are close to lithostatic levels rather than the hydrostatic levels that had earlier been assumed. High fluid pressures would reduce fault strength by lowering the effective stress across the fault. (A third model [*Brune et al.*, 1993; *Andrews and Ben-Zion*, 1997] involves fault motion by slip pulses, in which most of the slip occurs at low normal stresses while the fault surfaces are separated, thus reducing frictional heat generation. Because our data for serpentinite have no bearing on this hypothesis, it is not considered further in this paper.) Our results suggest that no variety of serpentine will be weak enough at hydrostatic fluid pressures to satisfy the constraints on fault strength described above. Lizardite and antigorite serpentinites are relatively strong at room temperature, and their strength is at least slightly greater at elevated temperatures and pressures (Figure 6). Metasomatic alteration of antigorite serpentinite to produce the impure gouge used in this study reduces the strength relative to pure antigorite, but the modified

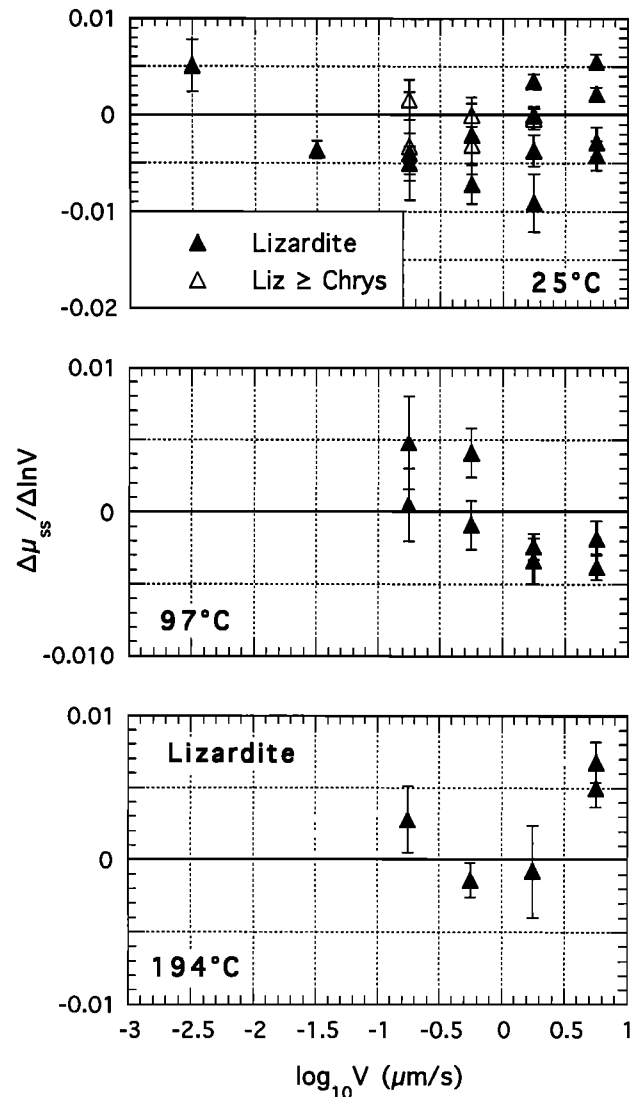


Figure 13. Variation in steady state coefficient of friction with changing axial velocity at 100 MPa effective normal stress for the lizardite gouge at 25–194°C and for the mixed gouge containing lizardite and chrysotile at 25°C.

gouge is as strong as lizardite. The alteration assemblage (Table 1) is fairly typical for such materials [Mumpton and Thompson, 1975]; therefore the strength of that gouge may be representative of altered antigoritic serpentinite.

Based on its low room temperature coefficient of friction (Figure 5), chrysotile was a possible candidate to explain the apparent weakness of serpentinite-bearing sections of the San Andreas fault. At shallow depths of burial (≤ 3 km), the coefficient of friction of chrysotile may be as low as 0.1, which would satisfy all constraints on fault strength. At progressively deeper levels, however, μ increases dramatically as a function of both temperature and effective stress, becoming as strong as the other serpentine minerals at pressure-temperature conditions approaching its upper limit of stability. Moore *et al.* [1996b] calculated that the average shear strength of a chrysotile-filled fault zone (converting to antigorite at temperatures above 300°C [Evans *et al.*, 1976]) would be nearly 50 MPa, which is more than double the limiting strength imposed by heat flow data [Brune *et al.*, 1969; Lachenbruch and Sass, 1980]. Moore *et al.* [1996b] combined these calculations with the available strength data for other notably weak minerals and concluded that no known mineral or rock type of potential significance to the San Andreas fault zone would be weak enough to validate the first group of models described above. Instead, a model from the second group, invoking nearly lithostatic fluid pressures, or one that combines somewhat elevated fluid pressures with relatively weak gouge materials, would be a better choice for rationalizing a weak San Andreas fault.

Serpentinite-bearing fault sections may be especially conducive to the generation of high fluid pressures, through the formation of permeability barriers that trap fluids within the fault zone. Many natural serpentinite bodies show textural evidence for multiple episodes of metamorphic crystallization and vein formation, in response to the passage of hydrothermal fluids through the rocks [e.g., O'Hanley, 1996]. Such reactions could lead to the development of seal-bounded compartments within a fault [Moore *et al.*, 1996b]. Depending on the prevailing conditions of temperature, pressure, and fluid and rock chemistry, any of the serpentine minerals potentially could crystallize within fluid-filled faults. However, chrysotile is probably the most important seal-forming serpentine mineral in the upper 9–10 km of the seismogenic zone, as evidenced by the correlation between chrysotile abundance and the degree of shearing of serpentinites [Page, 1968; Coleman and Keith, 1971; Mumpton and Thompson, 1975]. Escartin *et al.* [1997] found that the brittle deformation of solid serpentinite samples is nondilatant and accommodated by shear microcracking, which, they suggest, may create a microcrack pattern that would also trap fluids within a fault zone.

Just as water may be important to the generation of low fault strength, so too does water play a role in the strength of individual minerals. The well-known weak minerals, vermiculite and montmorillonite, are swelling clays that can incorporate multiple layers of loosely bound water into their structures. Our investigation of chrysotile strength has demonstrated that strongly adsorbed water can also substantially weaken a mineral. This suggests that the ability of a mineral to adsorb water could be an indicator of its relative strength. For example, many phyllosilicate minerals, such as clays, adsorb some water [Deer *et al.*, 1962], which may contribute to their reduced strength relative to minerals such as quartz or feldspar.

At least three naturally occurring polytypes of chrysotile have been identified [O'Hanley, 1996], and the platy habit of lizardite allows for the formation of a much larger number of polytypes [Bailey, 1988; Bailey and Banfield, 1995]. The various polytypes of chrysotile and lizardite represent differences in the stacking order of the layers, which affects the symmetry of the crystal but should have little effect on strength. The available data support the hypothesis that different polytypes of a particular serpentine mineral have similar strengths. The experiment that we conducted on a sample of orthochrysotile gouge (Figure 5c) yielded a room temperature coefficient of friction identical to that of clinochrysotile, which also suggests that orthochrysotile adsorbs appreciable amounts of water. In the same way, the strength of serpentinite sample ALM-1 of Summers and Byerlee [1977a, b], whose X ray diffraction pattern is consistent with lizardite 6T [Moore *et al.*, 1996a], corresponds to that of other lizardite-rich samples (Figure 1). These results are of significance to fault zones, because Banfield *et al.* [1995] demonstrated that deformation can induce changes in the polytype of lizardite, as a result of shearing along the basal plane that shifts the alignment of the layers.

Distributing shear across a wide gouge zone cannot be invoked to substantially reduce the strength of serpentinite-bearing faults. In contrast to the room temperature velocity behavior of chrysotile (Figure 10), at elevated temperatures, its coefficient of friction is largely unaffected by velocity change at low velocities. If these trends continue to still lower velocities, then fault strength will correspondingly be independent of the width of the zone of shear. In addition, our textural observations indicate that shearing of all three gouge types is concentrated along narrow, slickenlined surfaces (Figure 8) at all temperatures tested, rather than distributed across the width of the gouge layer.

Based on their room temperature experiments on serpentinite, Reinen *et al.* [1991] proposed that serpentinite could be a cause of creep, in that large earthquakes would not be initiated in serpentinite-bearing faults because of the observed velocity-strengthening behavior at low velocities. They noted, however, that unstable slip initiated outside a serpentinite-bearing fault section could propagate through it, because serpentinite is velocity weakening at high velocities. Our velocity data at 97 and 194°C (Figures 10–13) suggest that the velocity-strengthening behavior of serpentinite is confined to a restricted range of velocities at a given temperature. Nevertheless, regimes of velocity-strengthening behavior apparently occur for all three gouge types at low to moderate velocities, which presumably could dampen an instability initiated within the creeping zone. However, the 281°C (9 km) experiment indicates the possibility that serpentinite is velocity weakening at deeper levels in the seismogenic zone. More thorough velocity studies on serpentinite, over an expanded range of velocity, temperature, and pressure conditions applicable to fault zones, are required to elucidate the role of serpentinite in generating fault creep. Another important question is the effect on sliding behavior of mixing serpentinite with other fault zone materials, as is observed in central California [Rymer, 1982].

Our results on the temperature and velocity dependence of serpentinite strength, particularly for chrysotile, point out the hazards of interpreting the behavior of materials at depth in a fault based solely on room temperature data. Serpentinite may

be an extreme example of the possible variations in mechanical properties accompanying temperature and pressure changes; even so, the properties of all important fault zone materials should be investigated under hydrothermal conditions to more closely simulate actual conditions at depth.

Conclusions

Our room temperature strength measurements of the three major serpentine varieties corroborate previous reports that lizardite and antigorite gouge are both relatively strong materials and at least twice as strong as chrysotile gouge. The low coefficient of friction of chrysotile is caused by its high adsorbed water content. When the adsorbed water is removed, chrysotile is as strong as the other serpentine varieties. The correlation between the adsorbed-water content of a mineral and its strength may warrant further investigation.

The coefficient of friction of all three serpentinite gouges increases at least slightly with increasing temperature. Metasomatically altered antigorite gouge has reduced strength compared to pure antigorite, but the altered gouge is as strong as lizardite- and illite-rich gouges. The coefficient of friction of chrysotile goes through a minimum of about 0.1 at temperatures near 100°C but increases substantially with further heating, such that chrysotile is essentially as strong as lizardite and antigorite at ~300°C. This trend suggests that chrysotile gradually loses its adsorbed-water content with progressive burial. A fault zone filled with any type of serpentinite gouge will be too strong to meet the limitations on San Andreas fault strength required by heat flow and stress orientation data if hydrostatic fluid pressures are assumed. Fluid pressures well above hydrostatic levels are a better explanation for producing a weak, serpentinite-rich fault zone. Serpentinites are highly reactive in the presence of hydrothermal fluids, and the crystallization of serpentine minerals, particularly chrysotile, in fractures and pore spaces may readily create permeability barriers that help to raise fluid pressures within a fault zone.

The velocity dependence of heated chrysotile gouge differs significantly from its room temperature behavior. The data for chrysotile may be explained by a band of velocity-strengthening behavior that migrates to higher velocities with increasing temperature; outside this band, μ is nearly independent of velocity change. The velocity dependence of heated antigorite and lizardite gouges may follow trends similar to that of chrysotile, but the smaller velocity range tested for these minerals precludes a definite correlation. The available data on velocity dependence do not rule out serpentinite as a means of stabilizing slip in fault zones, especially at shallow depths, although serpentinite may possibly become velocity weakening, and therefore capable of unstable slip, near the base of the seismogenic zone.

Acknowledgments. We thank R. G. Coleman for supplying some of the serpentinite samples used in this study and for sharing his expertise on serpentinite. L. A. Reinen and T. E. Tullis kindly furnished us with some of their little remaining serpentinite gouge sample T91N16. Richard A. Vance of KCAC, Inc. gave permission for two of us (D.E.M. and R.S.) to collect samples at the company's asbestos mine near New Idria, California; and E. C. Madlangbayan, mine superintendent, accompanied us to the mine. R. Mariner of the Water Resources Division of the U.S. Geological Survey allowed us to use the X ray diffractometer in his laboratory. N. Beeler and R. G. Coleman provided helpful reviews of an early version of the manuscript.

References

- Allen, C. R., The tectonic environments of seismically active and inactive areas along the San Andreas fault system, in *Proceedings of Conference on Geologic Problems of San Andreas Fault System*, edited by W. R. Dickinson and A. Grantz, *Stanford Univ. Publ. Geol. Sci.*, 11, 70–80, 1968.
- Andrews, D. J., and Y. Ben-Zion, Wrinkle-like slip pulse on a fault between different materials, *J. Geophys. Res.*, 102, 553–571, 1997.
- Bailey, S. W., X-ray diffraction identification of the polytypes of mica, serpentine, and chlorite, *Clays Clay Miner.*, 36, 193–213, 1988.
- Bailey, S. W., and J. F. Banfield, Derivation and identification of non-standard serpentine polytypes, *Am. Mineral.*, 80, 1104–1115, 1995.
- Banfield, J. F., S. W. Bailey, W. W. Barker, and R. C. Smith, II, Complex polytypism: Relationships between serpentine structural characteristics and deformation, *Am. Mineral.*, 80, 1116–1131, 1995.
- Bird, P., Hydration-phase diagrams and friction of montmorillonite under laboratory and geologic conditions, with implications for shale compaction, slope stability, and strength of fault gouge, *Tectonophysics*, 107, 235–260, 1984.
- Bonatti, E., Serpentinite protrusions in the oceanic crust, *Earth Planet. Sci. Lett.*, 32, 107–113, 1976.
- Brune, J. N., T. L. Henyey, and R. F. Roy, Heat flow, stress, and rate of slip along the San Andreas fault, California, *J. Geophys. Res.*, 74, 3821–3827, 1969.
- Brune, J. N., S. Brown, and P. A. Johnson, Rupture mechanism and interface separation in foam rubber models of earthquakes: A possible solution to the heat flow paradox and the paradox of large overthrusts, *Tectonophysics*, 218, 59–67, 1993.
- Christensen, N. I., The abundance of serpentinites in the oceanic crust, *J. Geol.*, 80, 709–719, 1972.
- Coleman, R. G., Petrologic and geophysical nature of serpentinites, *Geol. Soc. Am. Bull.*, 82, 897–918, 1971.
- Coleman, R. G., and T. E. Keith, A chemical study of serpentinitization — Burro Mountain, California, *J. Petrol.*, 12, 311–328, 1971.
- Craw, D., C. A. Landis, and P. I. Kelsey, Authigenic chrysotile formation in the matrix of Quaternary debris flows, northern Southland, New Zealand, *Clays Clay Miner.*, 35, 43–52, 1987.
- Deer, W. A., R. A. Howie, and J. Zussman, *Rock-forming Minerals*, vol. 3, *Sheet Silicates*, pp. 170–190, John Wiley, New York, 1962.
- Dengo, C. A., and J. M. Logan, Implications of the mechanical and frictional behavior of serpentinite to seismogenic faulting, *J. Geophys. Res.*, 86, 10,771–10,782, 1981.
- Engeln, J. F., D. A. Wiens, and S. Stein, Mechanisms and depths of Atlantic transform earthquakes, *J. Geophys. Res.*, 91, 548–577, 1986.
- Escartin, J., G. Hirth, and B. Evans, Non-dilatant brittle deformation of serpentinites: Implications for Mohr-Coulomb theory and the strength of faults, *J. Geophys. Res.*, 102, 2897–2913, 1997.
- Evans, B. W., W. Johannes, H. Oterdoom, and V. Trommsdorff, Stability of chrysotile and antigorite in the serpentine multisystem, *Schweiz. Miner. Petrogr. Mitt.*, 56, 79–93, 1976.
- Faust, G. T., and J. J. Fahey, The serpentine group minerals, *U.S. Geol. Surv. Prof. Pap.*, 384-A, 91 pp., 1962.
- Francis, T. J. G., Serpentinization faults and their role in the tectonics of slow spreading ridges, *J. Geophys. Res.*, 86, 11,616–11,622, 1981.
- Giese, R. F., Jr., Kaolin minerals: Structures and stabilities, in *Hydrous Phyllosilicates (Exclusive of Micas)*, *Rev. Mineral.*, vol. 19, edited by S. W. Bailey, pp. 29–66, Mineral. Soc. of Am., Washington, D.C., 1988.
- Irwin, W. P., and I. Barnes, Effect of geologic structure and metamorphic fluids on seismic behavior of the San Andreas fault system in central and northern California, *Geology*, 3, 713–716, 1975.
- Iwata, K., D. Lockner, D. Moore, J. Byerlee, and H. Tanaka, Dependence of chrysotile strength on temperature and effective normal stress, *Eos Trans AGU*, 77 (46), Fall Meet. Suppl., F744, 1996.
- Lachenbruch, A. H., and J. H. Sass, Thermo-mechanical aspects of the San Andreas fault system, in *Proceedings of the Conference on the Tectonic Problems of the San Andreas Fault System*, edited by R. L. Kovach and A. Nur, *Stanford Univ. Publ. Geol. Sci.*, 13, 192–205, 1973.
- Lachenbruch, A. H., and J. H. Sass, Heat flow and energetics of the San Andreas fault zone, *J. Geophys. Res.*, 85, 6185–6222, 1980.
- Logan, J. M., and K. A. Rauenzahn, Frictional dependence of gouge mixtures of quartz and montmorillonite on velocity, composition and fabric, *Tectonophysics*, 144, 87–108, 1987.

- Moore, D. E., R. Summers, and J. D. Byerlee, Strengths of clay and non-clay fault gouges at elevated temperatures and pressures, *Proc. U.S. Symp. Rock Mech.*, 24th, 489–500, 1983.
- Moore, D. E., R. Summers, and J. D. Byerlee, The effects of sliding velocity on the frictional and physical properties of heated fault gouge, *Pure Appl. Geophys.*, 124, 31–52, 1986.
- Moore, D. E., R. Summers, and J. D. Byerlee, Sliding behavior and deformation textures of heated illite gouge, *J. Struct. Geol.*, 11, 329–342, 1989.
- Moore, D. E., D. A. Lockner, R. Summers, J. D. Byerlee, and S. Ma, Sample characterization and strength measurements of serpentinite gouges, *U.S. Geol. Surv. Open File Rep.*, 96–702, 88 pp., 1996a.
- Moore, D. E., D. A. Lockner, R. Summers, S. Ma, and J. D. Byerlee, Strength of chrysotile-serpentinite gouge under hydrothermal conditions: Can it explain a weak San Andreas fault?, *Geology*, 24, 1041–1044, 1996b.
- Morrow, C. A., L. Q. Shi, and J. D. Byerlee, Strain hardening and strength of clay-rich fault gouges, *J. Geophys. Res.*, 87, 6771–6780, 1982.
- Morrow, C., B. Radney, and J. Byerlee, Frictional strength and the effective pressure law of montmorillonite and illite clays, in *Fault Mechanics and Transport Properties of Rocks*, edited by B. Evans and T.-F. Wong, pp. 69–88, Academic, San Diego, Calif., 1992.
- Mount, V. S., and J. Suppe, State of stress near the San Andreas fault: Implications for wrench tectonics, *Geology*, 15, 1143–1146, 1987.
- Mumpton, F. A., and C. S. Thompson, Mineralogy and origin of the Coalinga asbestos deposit, *Clays Clay Miner.*, 23, 131–143, 1975.
- O'Hanley, D. S., Fault-related phenomena associated with hydration and serpentine recrystallization during serpentinitization, *Can. Mineral.*, 29, 21–35, 1991.
- O'Hanley, D. S., *Serpentinites, Records of Tectonic and Petrological History*, 277 pp., Oxford Univ. Press, New York, 1996.
- O'Hanley, D. S., and F. J. Wicks, Conditions of formation of lizardite, chrysotile, and antigorite, Cassiar, British Columbia, *Can. Mineral.*, 33, 753–773, 1995.
- O'Hanley, D. S., J. V. Chernosky Jr., and F. W. Wicks, The stability of lizardite and chrysotile, *Can. Mineral.*, 27, 483–493, 1989.
- Oldenburg, D. W., and J. N. Brune, An explanation for the orthogonality of ocean ridges and transform faults, *J. Geophys. Res.*, 80, 2575–2585, 1975.
- Page, N. J., Chemical differences among the serpentine "polymorphs", *Am. Mineral.*, 53, 201–215, 1968.
- Paterson, M. S., *Experimental Rock Deformation—The Brittle Field*, 254 pp., Springer-Verlag, New York, 1978.
- Raleigh, C. B., and M. S. Paterson, Experimental deformation of serpentinite and its tectonic implications, *J. Geophys. Res.*, 70, 3965–3985, 1965.
- Reinen, L. A., and T. E. Tullis, Microstructural evidence of strain localization and distributed strain in serpentine friction experiments, *Eos Trans. AGU*, 76(46), Fall Meet. Suppl., F560, 1995.
- Reinen, L. A., J. D. Weeks, and T. E. Tullis, The frictional behavior of serpentinite: Implications for aseismic creep on shallow crustal faults, *Geophys. Res. Lett.*, 18, 1921–1924, 1991.
- Reinen, L. A., T. E. Tullis, and J. D. Weeks, Two-mechanism model for frictional sliding of serpentinite, *Geophys. Res. Lett.*, 19, 1535–1538, 1992.
- Reinen, L. A., T. E. Tullis, and J. D. Weeks, A mechanism for weak, creeping faults, *Eos Trans. AGU*, 74(43), Fall Meet. Suppl., F589, 1993.
- Reinen, L. A., J. D. Weeks, and T. E. Tullis, The frictional behavior of lizardite and antigorite serpentinites: Experiments, constitutive models, and implications for natural faults, *Pure Appl. Geophys.*, 143, 317–358, 1994.
- Rutter, E. H., and K. H. Brodie, Experimental "syntectonic" dehydration of serpentinite under conditions of controlled pore water pressure, *J. Geophys. Res.*, 93, 4907–4932, 1988.
- Rymer, M. J., Structural framework of the San Andreas fault zone along Mustang Ridge, Monterey County, California, *Geol. Soc. Am. Abstr. Programs*, 14, 229, 1982.
- Scott, D. R., D. A. Lockner, J. D. Byerlee, and C. G. Sammis, Triaxial testing of Lopez fault gouge at 150 MPa mean effective stress, *Pure Appl. Geophys.*, 142, 749–775, 1994.
- Summers, R., and J. Byerlee, A note on the effects of fault gouge composition on the stability of frictional sliding, *Int. J. Rock Mech. Min. Sci.*, 14, 155–160, 1977a.
- Summers, R., and J. Byerlee, Summary of results of frictional sliding studies, at confining pressures up to 6.98 kb, in selected rock materials, *U.S. Geol. Surv. Open File Rep.*, 77-142, 129 pp., 1977b.
- Thatcher, W., Present-day crustal movements and the mechanics of cyclic deformation, in *The San Andreas Fault System, California*, edited by R. E. Wallace, *U.S. Geol. Surv. Prof. Pap.*, 1515, 189–205, 1990.
- Wang, C.-Y., On the constitution of the San Andreas fault zone in central California, *J. Geophys. Res.*, 89, 5858–5866, 1984.
- Wenner, D. B., and H. P. Taylor Jr., Temperatures of serpentinitization of ultramafic rocks based on O^{18}/O^{16} fractionation between coexisting serpentine and magnetite, *Contrib. Mineral. Petrol.*, 32, 165–185, 1971.
- Whittaker, E. J. W., and J. Zussman, The characterization of serpentine minerals by X-ray diffraction, *Mineral. Mag.*, 31, 107–126, 1956.
- Wicks, F. J., and D. S. O'Hanley, Serpentine minerals: Structures and petrology, in *Hydrous Phyllosilicates (Exclusive of Micas)*, *Rev. Mineral.*, vol. 19, edited by S. W. Bailey, pp. 91–167, Mineral. Soc. of Am., Washington, D.C., 1988.
- Wilcock, W. S. D., G. M. Purdy, and S. C. Solomon, Microearthquake evidence for extension across the Kane transform fault, *J. Geophys. Res.*, 95, 15,439–15,462, 1990.
- Young, G. J., and F. H. Healey, The physical structure of asbestos, *J. Phys. Chem.*, 58, 881–884, 1954.
- Zoback, M. D., et al., New evidence on the state of stress of the San Andreas fault system, *Science*, 238, 1105–1111, 1987.

J. D. Byerlee, D. A. Lockner, D. E. Moore, and R. Summers, U.S. Geological Survey, 345 Middlefield Road, MS 977, Menlo Park, CA 94025. (e-mail: jbyerlee@isdmnl.wr.usgs.gov; dlockner@isdmnl.wr.usgs.gov; dmoore@isdmnl.wr.usgs.gov; rsummers@isdmnl.wr.usgs.gov)

Ma S., Institute of Geology, State Seismological Bureau, Beijing, China.

(Received October 4, 1996; revised March 25, 1997; accepted April 2, 1997.)